# Integrating MRI Volume and Plasma p-Tau217 for Amyloid Risk Stratification in Early-Stage Alzheimer Disease

Sohyun Yim, <sup>1</sup> Seongbeom Park, <sup>2</sup> Kyoungyoon Lim, <sup>2</sup> Heekyung Kang, <sup>1</sup> Daeun Shin, <sup>1</sup> Hyunjin Jo, <sup>1</sup> Hyemin Jang, <sup>3</sup> Michael W. Weiner, <sup>4</sup> Henrik Zetterberg, <sup>5,6,7,8,9,10</sup> Kaj Blennow, <sup>5,6,11,12</sup> Fernando Gonzalez-Ortiz, <sup>5,6</sup> Nicholas J. Ashton, <sup>5,13,14,15</sup> Sung Hoon Kang, <sup>16</sup> Jihwan Yun, <sup>17</sup> Min Young Chun, <sup>18,19</sup> Eun-Joo Kim, <sup>20</sup> Hee Jin Kim, <sup>1,21,22,23</sup> Duk L. Na, <sup>1,21</sup> Jun Pyo Kim, <sup>1,21</sup> Sang Won Seo, <sup>1,21,22,23,1\*</sup> and Kichang Kwak, <sup>2,2\*</sup> for the K-ROAD study and the Alzheimer's Disease Neuroimaging Initiative

Neurology® 2025;105:e213954. doi:10.1212/WNL.0000000000213954

#### Correspondence

Dr. Seo sangwonseo@empal.com or Dr. Kwak kichang.kwak@ beaubrain.bio

#### MORE ONLINE

**Supplementary Material** 

# **Abstract**

## **Background and Objectives**

Identifying  $\beta$ -amyloid  $(A\beta)$  positivity is crucial for selecting candidates for  $A\beta$ -targeted therapies in early-stage Alzheimer disease (AD). While  $A\beta$  PET is accurate, its high cost limits routine use. Plasma p-tau217 testing offers a less invasive option but also incurs additional costs. Structural brain MRI, routinely used in cognitive assessments, can identify features predictive of  $A\beta$  positivity without extra expense. We evaluated a 2-stage workflow integrating MRI-based features and plasma p-tau217 to efficiently predict  $A\beta$  PET positivity in early-stage AD.

#### **Methods**

This prospective cohort study included participants with mild cognitive impairment (MCI) or early Alzheimer-type dementia (ATD) from the Korea-Registries to Overcome Dementia and Accelerate Dementia Research (K-ROAD; Korea) and Alzheimer's Disease Neuroimaging Initiative (ADNI; US) cohorts. Eligible participants had a Clinical Dementia Rating score of 0.5, along with MRI, plasma p-tau217, and A $\beta$  PET data. A random forest classifier predicting A $\beta$  PET positivity was developed using MRI-based brain atrophy patterns and APOE  $\epsilon$ 4 status. Participants were stratified into low-risk, intermediate-risk, and high-risk groups; plasma p-tau217 testing was performed only in intermediate-risk individuals. Outcomes included positive predictive value (PPV), negative predictive value (NPV), and overall accuracy.

#### Results

A total of 807 K-ROAD participants (median age 72.0 years, 58.7% female) and 230 ADNI participants (median age 70.9 years, 49.1% female) were analyzed. Using a 95% sensitivity/specificity strategy, the low-risk group demonstrated NPVs of 94.7% (91.7%–97.7%, K-ROAD)

The Article Processing Charge was funded by the authors.

K-ROAD Coinvestigators are listed online at Neurology.org.

Data used in preparation of this article were obtained from the Alzheimer's Disease Neuroimaging Initiative (ADNI) database. As such, the investigators within the ADNI contributed to the design and implementation of ADNI and/or provided data but did not participate in analysis or writing of this report. A complete listing of ADNI investigators can be found in the Appendix at Neurology.org/N.

This is an open access article distributed under the terms of the Creative Commons Attribution-Non Commercial-No Derivatives License 4.0 (CCBY-NC-ND), where it is permissible to download and share the work provided it is properly cited. The work cannot be changed in any way or used commercially without permission from the journal.

<sup>\*</sup>These authors contributed equally to this article as co-corresponding authors.

<sup>&</sup>lt;sup>1</sup>Department of Neurology, Samsung Medical Center, Sungkyunkwan University School of Medicine, Seoul, South Korea; <sup>2</sup>BeauBrain Healthcare, Inc., Seoul, South Korea; <sup>3</sup>Department of Neurology, Seoul National University Hospital, Seoul National University Oflege of Medicine, South Korea; <sup>4</sup>Department of Radiology and Biomedical Imaging, University of California, San Francisco; <sup>5</sup>Department of Psychiatry and Neurochemistry, Institute of Neuroscience and Physiology, The Sahlgrenska Academy at the University of Gothenburg, Sweden; <sup>6</sup>Clinical Neurochemistry Laboratory, Sahlgrenska University Hospital, Mölndal, Sweden; <sup>7</sup>Department of Neurodegenerative Disease, UCL Institute of Neurology, Queen Square, London, United Kingdom; <sup>8</sup>UK Dementia Research Institute, UCL, London, United Kingdom; <sup>9</sup>Hong Kong Center for Neurodegenerative Diseases, Clear Water Bay, Hong Kong, China; <sup>10</sup>Wisconsin Alzheimer's Disease Research Center, University of Wisconsin School of Medicine and Public Health, Madison; <sup>11</sup>Paris Brain Institute, ICM, Pitié-Salpêtrière Hospital, Sorbonne University, France; <sup>12</sup>Neurodegenerative Disorder Research Center, Division of Life Sciences and Medicine, and Department of Neurology, Institute on Aging and Brain Disorders, University of Ceince and Technology of China and First Affiliated Hospital of USTC, Hefei, China; <sup>13</sup>King's College London, Institute of Psychiatry, Psychology and Neuroscience Maurice Wohl Institute Clinical Neuroscience Institute, United Kingdom; <sup>14</sup>MIHR Biomedical Research Centre for Mental Health and Biomedical Research Unit for Dementia at South London and Maudsley NHS Foundation, United Kingdom; <sup>15</sup>Centre for Age-Related Medicine, Stavanger University Hospital, Norway; <sup>16</sup>Department of Neurology, Korea University Guro Hospital, Korea University College of Medicine, Seoul, South Korea; <sup>17</sup>Department of Neurology, Yongin Severance Hospital, Yonsei University Guro Hospital, South Korea; <sup>18</sup>Department of Neurology, Yongin Severance Hospital, Yonsei University Hospital, Pus

# Glossary

Aβ = β-amyloid; AD = Alzheimer disease; ADNI = Alzheimer's Disease Neuroimaging Initiative; ATD = Alzheimer-type dementia; AUC = area under the curve; CDR = Clinical Dementia Rating; CDR-SOB = CDR-Sum of Boxes; CL = Centiloid; FBB = 18F-florbetaben; FBP = 18F-florbetapir; FMM = 18F-flutemetamol; IQR = interquartile range; K-ROAD = Korea-Registries to Overcome Dementia and Accelerate Dementia Research; LV = lateral ventricle; MCI = mild cognitive impairment; NPV = negative predictive value; PPV = positive predictive value; Se = sensitivity; SIMOA = Single-Molecule Array; Sp = specificity; SUVR = standardized uptake value ratio.

and 99.0% (97.0%–100.0%, ADNI). The high-risk group showed PPVs of 97.6% (95.9%–99.3%, K-ROAD) and 98.8% (96.5%–100.0%, ADNI). Intermediate-risk groups comprised 33.3% (K-ROAD) and 20.9% (ADNI) of participants. Plasma p-tau217 testing in intermediate-risk groups yielded PPVs of 92.5% (88.7%–96.3%, K-ROAD) and 90.0% (79.0%–100.0%, ADNI) and NPVs of 83.1% (75.0%–91.2%, K-ROAD) and 83.3% (66.1%–100.0%, ADNI). The overall workflow accuracy was 94.2% (92.6%–95.8%, K-ROAD) and 96.5% (94.1%–98.9%, ADNI).

#### **Discussion**

The 2-stage diagnostic workflow integrating MRI-based risk stratification and plasma p-tau217 testing accurately identified individuals with  $A\beta$  PET positivity in early-stage AD, substantially reducing the need for additional biomarker testing. However, the generalizability may be limited by modest incremental improvement over baseline models and limited racial and ethnic diversity.

## Introduction

Alzheimer disease (AD) is characterized by 2 key pathologic hallmarks: extracellular  $\beta$ -amyloid (A $\beta$ ) plaques and intracellular tau neurofibrillary tangles. These pathologies result in neurodegeneration, leading to regional brain atrophy observable in vivo through structural imaging. Notable changes include atrophy in the medial temporal lobe and posterior parietal cortex, which often manifest as sulcal widening and ventricular enlargement, particularly in the temporal horns of the lateral ventricles (LVs). Recently, A $\beta$ -targeted therapies have shown promise in modifying the disease course in its early stages. Consequently, detecting A $\beta$  accumulation in vivo has become critical for identifying patients with mild cognitive impairment (MCI) or early Alzheimer-type dementia (ATD) who may benefit from these therapies.

Currently, A $\beta$  accumulation is most reliably assessed using amyloid PET imaging <sup>12-14</sup> or CSF testing. <sup>15-17</sup> However, despite their high accuracy, these modalities are costly, invasive, and not universally accessible, limiting their utility in routine clinical practice. <sup>18,19</sup> By contrast, structural brain imaging such as MRI or CT is a mandatory diagnostic tool for evaluating patients with cognitive impairment because it is essential for excluding alternative causes such as brain tumors, strokes, or hydrocephalus. <sup>20,21</sup> MRI is generally preferred over CT in clinical practice because of its superior sensitivity to subtle atrophy and its ability to rule out multiple differential diagnoses with a single scan, although it cannot be performed in patients with contraindications. Moreover, MRI-derived brain atrophy patterns, including medial temporal atrophy and related structural changes, correlate significantly with A $\beta$  accumulation. <sup>22-25</sup> This provides an opportunity to

screen for  $A\beta$  positivity using existing imaging data, eliminating the need for additional costly or invasive procedures.

However, relying solely on MRI findings poses challenges, particularly in ambiguous cases where structural changes are subtle or overlap with non-AD conditions. A gray zone remains, where A $\beta$  positivity cannot be clearly classified based on MRI findings alone. Solve To address this uncertainty, a risk stratification framework is necessary, where MRI is used to identify low-risk and high-risk individuals while intermediate-risk individuals undergo confirmatory testing. Plasma p-tau217, a biomarker reflective of tau-related neurodegeneration, has emerged as a highly accurate tool for detecting A $\beta$  accumulation. Its potential utility as a confirmatory test within a 2-stage workflow makes it an ideal complement to MRI, addressing diagnostic uncertainty in intermediate-risk cases.

In this study, we aim to evaluate a 2-stage diagnostic workflow integrating MRI-based brain atrophy assessments and plasma p-tau217 testing to predict  $A\beta$  PET positivity in patients with early-stage AD, with validation across different clinical cohorts to ensure broader applicability. By combining these modalities, the study seeks to address diagnostic uncertainty in intermediate-risk groups, optimize resource allocation, and provide a scalable framework for improving early diagnosis in clinical practice.

# Methods

#### **Participants**

This study was designed as a prospective cohort study conducted at a tertiary hospital in South Korea. Participants were

recruited from the Korea-Registries to Overcome Dementia and Accelerate Dementia Research (K-ROAD) project in South Korea,<sup>34</sup> which is a global partner of the Alzheimer's Disease Neuroimaging Initiative (ADNI). This study used a convenience sampling approach. Individuals diagnosed with MCI and early-stage ATD, between 55 and 90 years, were included if they had undergone testing for APOE genotype, Aß PET imaging, and 3D T1-weighted MRI. A comprehensive dementia assessment was conducted for all participants, including clinical interviews, detailed neurologic examinations, and standardized neuropsychological assessments using the Seoul Neuropsychological Screening Battery. 35 Especially, verbal memory was assessed using the Seoul Verbal Learning Test and visual memory using the Rey Complex Figure Test, including immediate recall, delayed recall, and recognition. MCI diagnosis was established using Petersen clinical criteria for amnestic MCI with the following modifications<sup>36,37</sup>: subjective memory concerns reported by the patient or caregiver, preserved functional independence in daily activities, objective cognitive performance falling below -1.0 SD of age-matched and education-matched norms in neuropsychological testing, and not being demented. The diagnosis of early-stage ATD was based on the 2011 National Institute on Aging and Alzheimer's Association criteria, 38 requiring a Clinical Dementia Rating (CDR) score of 0.5. Individuals with cognitive impairment due to secondary causes, as confirmed by laboratory tests for vitamin B12 deficiency; syphilis serology; and thyroid, renal, or hepatic dysfunction, were excluded. Participants with major structural brain lesions, such as territorial infarction, intracranial hemorrhage, brain tumors, or extensive white matter hyperintensities, classified according to the modified Fazekas ischemic scale, <sup>39</sup> were also excluded. Furthermore, those diagnosed with other neurodegenerative diseases, such as progressive supranuclear palsy, corticobasal syndrome, frontotemporal dementia, or dementia with Lewy body/Parkinson disease, were not included. To ensure high statistical power, all eligible participants who met the inclusion and exclusion criteria and had complete data for the required biomarkers were included in the study. A detailed participant selection process is illustrated in eFigure 1.

For replication, an external cohort was drawn from ADNI, a widely used, publicly available data set consisting mainly of non-Hispanic Whites, led by principal investigator Michael Weiner. Individuals with MCI and early-stage ATD with a CDR score of 0.5 and available plasma p-tau217 measurements were included in this study (eFigure 1). Detailed inclusion and exclusion criteria for ADNI participants can be accessed on the official ADNI website.<sup>40</sup>

# Aβ PET Acquisition and Determination of Aβ Positivity

Aß PET scans were acquired using either 18F-florbetaben (FBB) or 18F-flutemetamol (FMM) tracer to assess amyloid deposition in the brain. Following ligand manufacturer-recommended guidelines, dynamic 20-minute PET imaging,

consisting of four 5-minute frames, was performed 90 minutes after the injection of a mean dose of 311.5 MBq FBB or 185 MBq FMM. PET images were aligned with each participant's MRI scan and spatially normalized to the Montreal Neurological Institute-152 standard using the appropriate transformation matrix. The gray matter of the brain was segmented into 116 anatomical areas using the automated anatomical labeling atlas. Standardized uptake value ratios (SUVRs) were computed using the cerebellum as the reference region, with regional masks obtained from the Global Alzheimer's Association Interactive Network website. Ab burden was quantified using BeauBrain Amylo software, which implements image processing methodologies based on the Centiloid (CL) scale.

For ADNI participants, A $\beta$  PET scans were acquired using 18F-florbetapir (FBP), with 20-minute dynamic acquisition (four 5-minute frames) occurring between 50 and 70 minutes after injection of 10.0 mCi of FBP. ADNI's standardized image pipeline included frame co-registration, motion correction, and intensity normalization to ensure data consistency across imaging sites. Full details of the T1 and PET acquisition parameters and image processing steps are listed on the ADNI website. A previously validated transformation equation was applied to convert SUVR values to CL units. A threshold of 20 CL was used to define A $\beta$  PET positivity across both K-ROAD and ADNI cohorts. The assessment of the A $\beta$  PET status was blinded to the participants' clinical information, MRI-based brain atrophy, and plasma p-tau217 result.

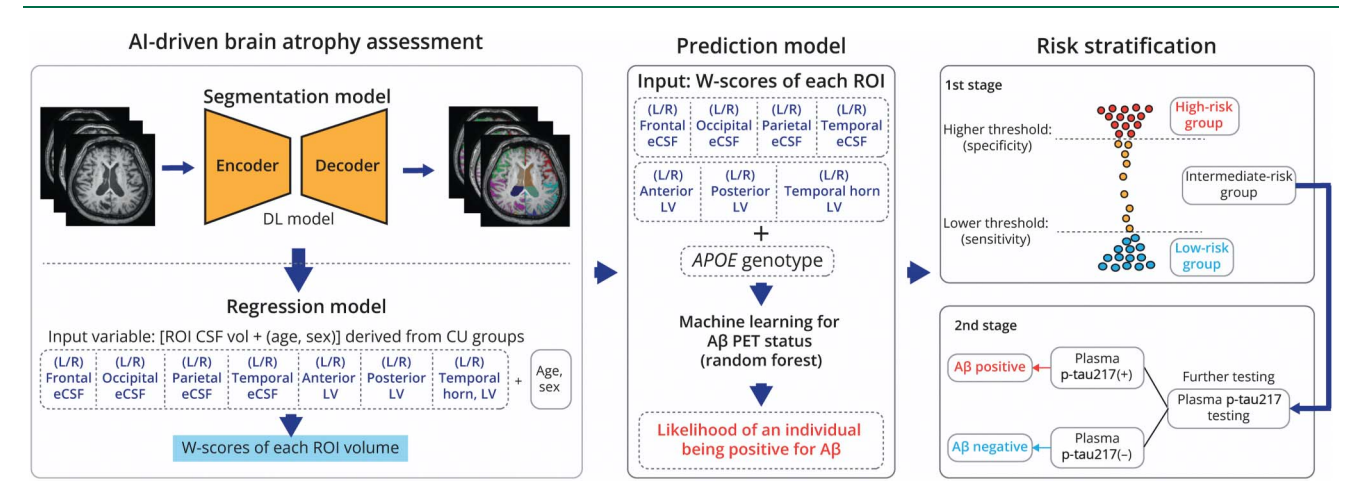
#### **Brain MRI Image Preprocessing**

In the K-ROAD cohort, high-resolution 3D T1 turbo field-echo MRI sequences were obtained using a 3.0T Philips Achieva scanner (Philips Healthcare, Andover, MA). Acquisition parameters included a sagittal slice thickness of 1.0 mm with 50% overlap and a reconstructed matrix size of 480 × 480 pixels over a 240-mm field of view. ADNI participants underwent structural MRI using 3.0T MRI scanners, with either inversion recovery–fast spoiled gradient-recalled or magnetization-prepared rapid gradient-echo sequences. Full details of the T1-weighted acquisition and processing protocols for ADNI are available on the official website.

#### **Al-Driven Brain Atrophy Assessment**

Figure 1 illustrates the framework used in this study. An AI-based brain MRI analysis was implemented using BeauBrain Morph software, which provides quantitative assessment of brain atrophy by segmenting CSF regions on MRI scans. A 2D nnUNet segmentation model<sup>43</sup> was used, and performance was evaluated using 5-fold cross-validation. Preprocessed images underwent further refinement with the default nnUNet preprocessing pipeline before training. The model was trained with a leaky rectified linear unit as the activation function, an objective function combining Dice loss and cross-entropy loss, and stochastic gradient descent as the optimizer. The learning rate was set to 1e-2, with a weight

Figure 1 Proposed Framework



The framework illustrates the results of an Al-powered brain MRI analysis that assesses brain atrophy using quantitative information from MRI scans. The 2-step framework for  $A\beta$  PET status classification aims to minimize additional confirmatory tests while ensuring accurate patient stratification. In the first step, a random forest model incorporating  $APOE \in A$  status and regional CSF volume predicts  $A\beta$  PET positivity, stratifying participants into 3 risk categories. In the second step, plasma p-tau217 testing is applied exclusively to the intermediate-risk group to refine predictions and facilitate risk-based decision making. \*The classification of  $A\beta$ -positive and  $A\beta$ -negative cases is determined based on  $A\beta$  PET status.  $A\beta = \beta$ -amyloid;  $A\beta = \beta$ -

decay of 3e-5. Training was conducted over 200 epochs with a batch size of 64. In addition, to facilitate cross-cohort comparisons, we standardized regional brain volumes using W-scores, referencing cognitively unimpaired participants (n = 936; age range 65.0-76.0 years; 61.5% female) in theK-ROAD cohort, while accounting for age and sex differences. We prioritized CSF spaces for brain atrophy assessment because of their strong intensity contrast with adjacent tissues, which reduces vendor-related variability and enhances reproducibility. These measures align with regions commonly used in clinical visual assessments by radiologists and neurologists, improving their applicability. In addition, this approach facilitates the use of 2D T1 MRI and CT scans, making it more suitable for real-world diagnostic settings. The analysts were blinded to the participants' clinical information and Aβ PET status. This AI-driven method was chosen because of its high diagnostic precision, ability to accommodate data from multiple MRI vendors, and significant reduction of the time and potential for human error inherent in manual segmentation. The software program automatically identifies 14 specific CSF regions, including the left and right CSF areas of the frontal, occipital, parietal, and temporal lobes, as well as the anterior LVs, posterior LVs, and temporal horns of LVs adjacent to the hippocampus.

# Plasma Collection and Processing for p-Tau217 Analysis

Blood samples from the K-ROAD cohort were collected from each participant in tubes containing 0.5M EDTA and mixed for 5 minutes. The samples were then centrifuged at 1,300g for 10 minutes to separate plasma, which was subsequently aliquoted into 5 or 10 vials, each containing 0.3 mL of plasma. These plasma samples were stored at  $-75^{\circ}$ C, following the

National Biobank of the Republic of Korea's guidelines for human biospecimen storage and registration. The frozen plasma samples were then transported under -70°C conditions to the Department of Psychiatry and Neurochemistry at the University of Gothenburg, where plasma p-tau217 concentrations were quantified using the commercial ALZpath p-Tau217 immunoassay on the Single-Molecule Array (SIMOA) HD-X instrument. This system, developed by Quanterix (Billerica, MA), uses a paramagnetic microbeadbased sandwich ELISA approach. The laboratory personnel were blinded to the participants' clinical diagnoses and Aβ PET status. For the ADNI cohort, plasma samples were processed following their standardized protocol and plasma p-tau217 analysis was conducted using the same ALZpath p-Tau217 immunoassay on the SIMOA HD-X instrument. While both cohorts used the ALZpath assay on the SIMOA instrument, K-ROAD samples were analyzed at the University of Gothenburg, whereas ADNI samples were processed and analyzed by Quanterix.

# Development of a 2-Stage Workflow for Aβ Positivity Prediction

To predict A $\beta$  PET positivity, we developed a classifier using several machine learning models, such as support vector machine, logistic regression, and random forest model, with a base model (including only age, sex, and *APOE* &4 status) and W-scores of regional CSF volume as predictors (Figure 1). This algorithm was selected because of its superior classification performance compared with other machine learning models, such as support vector machine and logistic regression (eFigure 2). Probabilities of A $\beta$  positivity were calculated based on brain atrophy and APOE &4 status, and a 2-stage diagnostic approach was established for risk

stratification. In the first stage, participants were classified into low-risk, intermediate-risk, and high-risk groups based on brain atrophy model-derived probabilities of Aß PET positivity. Thresholding strategies were defined using lower probability thresholds (90%, 95%, and 97.5% sensitivity [Se]) to minimize false negatives and higher probability thresholds (90%, 95%, and 97.5% specificity [Sp]) to reduce false positives. For example, thresholds were set to achieve 95% Se with 95% Sp for both MCI and ATD. For each thresholding strategy, the prevalence of AB PET negativity in the low-risk group and Aß PET positivity in the high-risk group was calculated. In the second stage, additional Aß biomarker testing with plasma p-tau217 measurements was simulated exclusively for intermediate-risk participants identified in the first step. Plasma p-tau217 was used to refine Aβ PET predictions in this subgroup, and the concordance between plasma biomarker levels and Aß PET status was assessed. The workflow's overall accuracy was calculated as the proportion of correct AB PET classifications across both stages, and the reduction in additional Aβ biomarker testing requirements was quantified to assess efficiency.

### **Statistical Analysis**

All statistical analyses were performed using R statistical software, version 4.0.2. 44 Descriptive statistics were computed for demographic and clinical characteristics, summarizing variables across participants. Group differences in continuous variables were assessed using analysis of variance, followed by Tukey post hoc comparisons when applicable. For categorical variables,  $\chi^2$  tests were performed to assess group differences, with Bonferroni correction applied for multiple pairwise comparisons where necessary. Predictive modeling was performed using Python version 3.8, with libraries such as scikit-learn<sup>45</sup> for machine learning tasks. The random forest classifier was trained and validated using k-fold crossvalidation (k = 5). For each fold, the model was trained on a subset of the data (training set) and its predictive performance was evaluated on the held-out test set, repeated across all 5 folds. Performance metrics, including accuracy, positive predictive value (PPV), and negative predictive value (NPV), were used to assess model effectiveness. To optimize hyperparameters, a grid search approach was used, fine-tuning key parameters such *n* estimators, max depth, min samples split, min\_samples\_leaf, and max\_features. In addition, a backward elimination approach was used to evaluate whether a base model (including only age, sex, and APOE & status) would provide preferable predictive performances to the full model (including only age, sex, and APOE & status and MRI measures). To maintain consistency throughout the predictive analysis, the same modeling approach was applied across all modeling-building processes. Thresholds for stratifying participants into risk groups were determined based on the desired Se and Sp levels (90%, 95%, and 97.5%). Plasma p-tau217 results were incorporated in the intermediate-risk group, and the concordance between plasma biomarker results and Aß PET status was evaluated. The overall accuracy of the 2-stage diagnostic workflow was calculated, and statistical significance was determined at a 2-tailed alpha level of 0.05.

# Standard Protocol Approvals, Registrations, and Participant Consents

This study was approved by the Institutional Review Board of Samsung Medical Center, and written informed consent was obtained from all participants and their caregivers in accordance with the Declaration of Helsinki. In addition, the use and publication of ADNI data were approved by the ADNI Data Sharing and Publications Committee.

### **Data Availability**

The data sets generated and analyzed during this study are available from the corresponding author on reasonable request.

## Results

### **Participant Characteristics**

The K-ROAD cohort included 807 participants with a median age of 72.0 years (58.7% female and 46.6% of APOE  $\epsilon$ 4 carriers) (Table 1). A $\beta$  PET positivity was observed in 64.3% of participants, and the median CDR-Sum of Boxes (CDR-SOB) score was 1.5. The median interval between the MRI scan and A $\beta$  PET imaging was 83.0 days (interquartile range [IQR] 23.0–163.5), and the median interval between the MRI scan and plasma p-tau217 measurement was 102.5 days (IQR 29.0–223.5). In addition, the independent set from ADNI included 230 participants with a median age of 70.9 years (49.1% female and 34.8% of APOE  $\epsilon$ 4 carriers) (Table 1). A $\beta$  PET positivity was observed in 52.6% of participants, with a median CDR-SOB score of 1.0.

# First-Stage Risk Stratification Using MRI-Based Brain Atrophy Patterns

MRI-based brain atrophy patterns were used in the first stage of a 2-stage diagnostic workflow to stratify participants into low-risk, intermediate-risk, and high-risk groups based on predicted probabilities of A $\beta$  PET positivity in K-ROAD (Figure 2A) and ADNI (Figure 2B) cohorts. The random forest model was selected because of its superior classification performance compared with other machine learning models (eFigure 2). Using both K-ROAD and ADNI data sets, adding MRI features to the base model (age + sex + APOE  $\epsilon$ 4) improved area under the curve (AUC) from 0.76 to 0.81 (p = 0.009) in the K-ROAD cohort and from 0.75 to 0.78 (p = 0.13) in the ADNI cohort (eTable 1).

In the K-ROAD cohort, for Se/Sp levels of 90%, 95%, and 97.5%, the NPVs in the low-risk group were 93.6%, 94.7%, and 96.3%, respectively, while the PPVs in the high-risk group were 93.3%, 97.6%, and 98.3%, respectively (Table 2). The proportion of patients categorized into the intermediate-risk group was 32.6%, 33.3%, and 46.7%, respectively. Among these, the Se/Sp level of 95% seemed most suitable, balancing high predictive values and a manageable size of the

Table 1 Demographics of Study Participants

	K-ROAD (n = 807)	ADNI (n = 230) 212 (92.2)	
Diagnosis, MCI, n (%)	671 (83.2)		
Age, y	72.0 (65.0–78.0)	70.9 (66.6–75.6)	
Sex, female, n (%)	474 (58.7)	113 (49.1)	
Race/ethnicity, n (%)			
Asian	807 (100.0)	3 (1.3)	
Non-Hispanic White	0	205 (89.1)	
Hispanic or Latino	0	22 (9.6)	
Education, y	12.0 (9.0–16.0)	16.0 (14.0–18.0)	
APOE ε4 carriers, n (%)	376 (46.6)	80 (34.8)	
Aβ PET positive, n (%)	519 (64.3)	121 (52.6)	
Plasma p-tau217, pg/mL <sup>a</sup>	0.73 (0.30–1.2)	0.43 (0.2-0.7)	
CDR-SOB	1.5 (1.0–3.0)	1.0 (0.5-2.0)	

Abbreviations:  $A\beta$  = amyloid- $\beta$ ; ADNI = Alzheimer's Disease Neuroimaging Initiative; CDR-SOB = Clinical Dementia Rating–Sum of Boxes; K-ROAD = Korea-Registries to Overcome Dementia and Accelerate Dementia Research; MCI = mild cognitive impairment; SIMOA = Single-Molecule Array. Data are presented as n (%) for categorical variables and median with interquartile range for continuous variables.

Statistical significance was defined as p < 0.05.

intermediate-risk group, which in turn helps reduce the overall cost of further testing (Figure 3). In the ADNI cohort, for Se/Sp levels of 90%, 95%, and 97.5%, the NPVs were 97.1%, 99.0%, and 100.0%, respectively, and the PPVs were 95.3%, 98.8%, and 98.8%, respectively (Table 2). The intermediate-risk group sizes were 8.7%, 20.9%, and 25.6%,

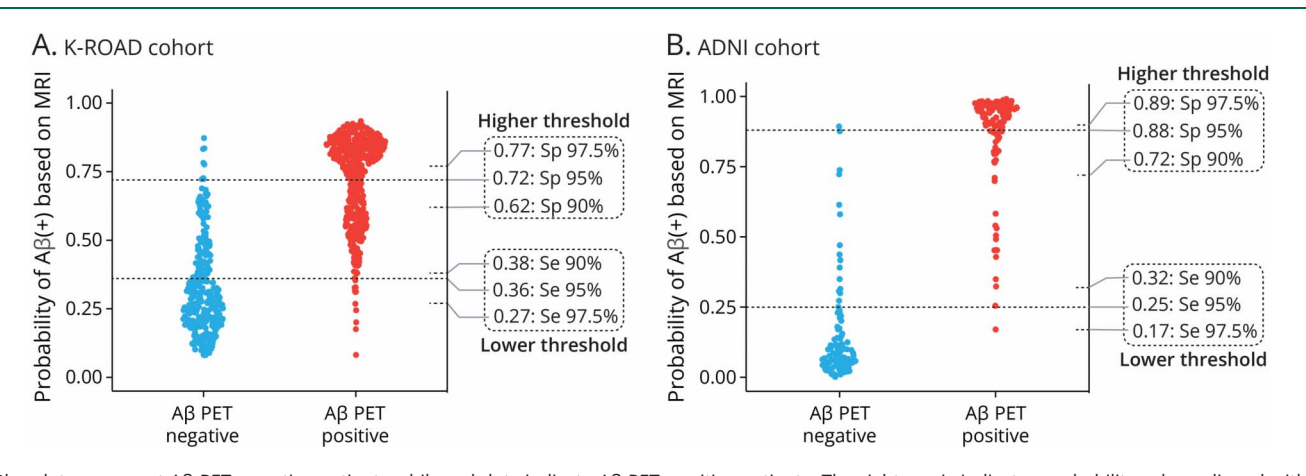
with 95% Se/Sp offering the best balance of accuracy and group size. Detailed demographic information for each of the 3 risk groups classified using the 95% Se/Sp strategy is provided in eTable 2. Because the model demonstrated good validation and calibration, probability thresholds were separately derived for the K-ROAD and ADNI data sets (eFigure 3).

# Second-Stage Refinement of Aβ PET Status Prediction With Plasma p-Tau217 Testing

In the second stage of the workflow, plasma p-tau217 testing was used to refine Aß PET status predictions for participants classified as intermediate risk based on the MRI-based model (Figure 4). Using the 95% Se/Sp strategy, which was identified as optimal in the first stage, 33.3% of K-ROAD participants were classified into the intermediate-risk group. Plasma p-tau217 testing achieved a PPV of 92.5% and a NPV of 83.1%, effectively improving diagnostic accuracy for these uncertain cases. The 95% Se/ Sp strategy also achieved the highest accuracy at 94.2% (95% CI 92.6%-95.8%) while reducing additional testing by 66.7% (Figure 4A). A sex-stratified analysis showed that the overall accuracy of the 2-stage workflow was comparable between men (93.7%) and women (94.5%). The proportion of participants classified as intermediate risk was also similar (36.9% in men, 30.8% in women), suggesting consistent performance across sexes (eFigure 4). In the ADNI cohort, 20.9% of participants were classified into the intermediate-risk group under the same 95% Se/Sp strategy. Plasma p-tau217 testing demonstrated a PPV of 90.0% for Aß PET positivity and an NPV of 83.3%, confirming the robustness and scalability of the 2-stage diagnostic workflow (Figure 4B).

We quantitatively assessed the incremental value of secondstage testing. In both K-ROAD and ADNI cohorts, the 2-step

**Figure 2** Distribution and Thresholds of Probability of Aβ (+) Based on MRI-Derived Brain Atrophy Patterns for the K-ROAD Cohort (A) and for the ADNI Cohort (B)



Blue dots represent A $\beta$  PET-negative patients while red dots indicate A $\beta$  PET-positive patients. The right y-axis indicates probability values aligned with evaluated 3 risk thresholds, accompanied by metrics defining Se (90%, 95%, 97.5%) and Sp (90%, 95%, 97.5%). A $\beta$  =  $\beta$ -amyloid; ADNI = Alzheimer's Disease Neuroimaging Initiative; K-ROAD = Korea-Registries to Overcome Dementia and Accelerate Dementia Research; Se = sensitivity; Sp = specificity.

<sup>&</sup>lt;sup>a</sup> Plasma p-tau217 levels were measured using the same SIMOA platform and ALZpath assay, but the differences between the cohorts may reflect site-specific variability (K-ROAD measurements were conducted at the University of Gothenburg and ADNI measurements at Quanterix).

Table 2 Accuracy and Risk Stratification for Aβ PET Positivity Across Threshold Strategies in K-ROAD and ADNI Cohorts

	K-ROAD			ADNI		
Risk groups	Participants in risk group, n (%)	Aβ PET status			Aβ PET status	
		Negativity, n (%)	Positivity, n (%)	Participants in risk group, n (%)	Negativity, n (%)	Positivity, n (%)
90% Se lower risk threshold/90% Sp higher risk threshold						
Low risk	218 (27.0)	204 (93.6)	14 (6.4)	103 (44.8)	100 (97.1)	3 (29)
Intermediate risk	188 (23.3)			20 (8.7)		
High risk	401 (49.7)	27 (6.7)	374 (93.3)	107 (46.5)	5 (4.7)	102 (95.3)
95% Se lower risk threshold/95% Sp higher risk threshold						
Low risk	208 (25.8)	197 (94.7)	11 (5.3)	97 (42.2)	96 (99.0)	1 (1.0)
Intermediate risk	269 (33.3)			48 (20.9)		
High risk	330 (40.9)	8 (2.4)	322 (97.6)	85 (37.0)	1 (1.2)	84 (98.8)
97.5% Se lower risk threshold/97.5% Sp higher risk threshold						
Low risk	136 (16.9)	131 (96.3)	5 (3.7)	87 (37.8)	87 (100)	0 (0)
Intermediate risk	377 (46.7)			59 (25.7)		
High risk	294 (36.4)	5 (1.7)	289 (98.3)	84 (36.5)	1 (1.2)	83 (98.8)

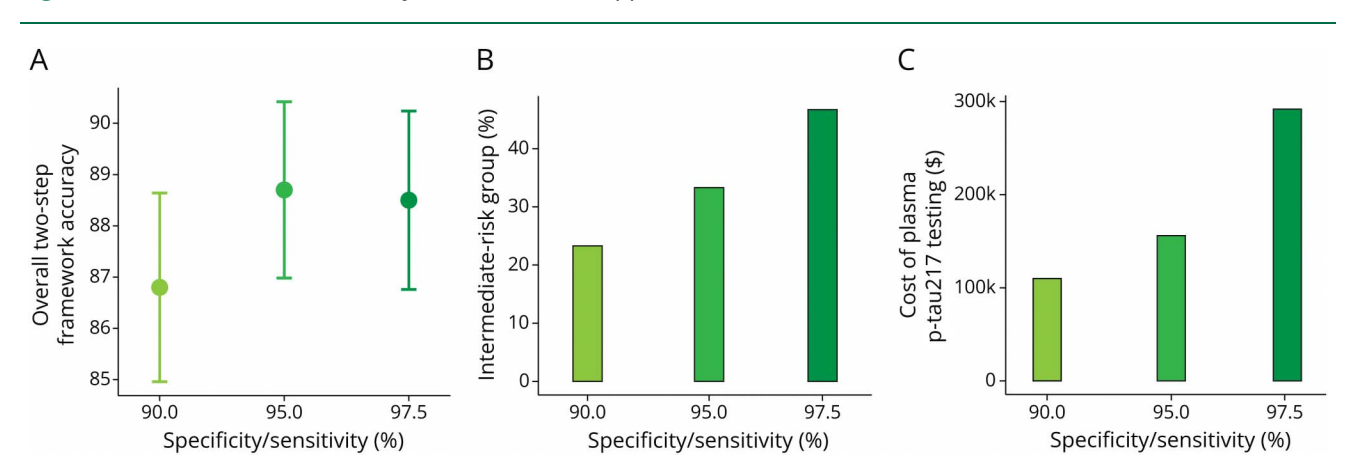
Abbreviations:  $A\beta$  = amyloid- $\beta$ ; ADNI = Alzheimer's Disease Neuroimaging Initiative; K-ROAD = Korea-Registries to Overcome Dementia and Accelerate Dementia Research; NPV = negative predictive value; PPV = positive predictive value; Se = sensitivity; Sp = specificity.

Data are presented as n or n (%). The first column indicates each of the evaluated strategies for MRI-based risk stratification, along with the corresponding low-risk, intermediate-risk, and high-risk groups for each strategy. The second column indicates the number of screened individuals assigned to each risk category, with the percentage of individuals in the intermediate-risk group shown in parentheses. The third and fourth columns indicate the  $A\beta$  PET status for low-risk, intermediate-risk, and high-risk groups. The percentage of  $A\beta$ -negative individuals in the low-risk group and the percentage of  $A\beta$ -negative individuals in the low-risk group and the percentage of  $A\beta$ -negative individuals in the low-risk group and the same structure for the ADNI cohort.

workflow significantly outperformed the 1-step model (K-ROAD AUC: 0.93 vs 0.82; ADNI AUC: 0.92 vs 0.80; DeLong test, p < 0.001 for both; Figure 5, A and B). In the

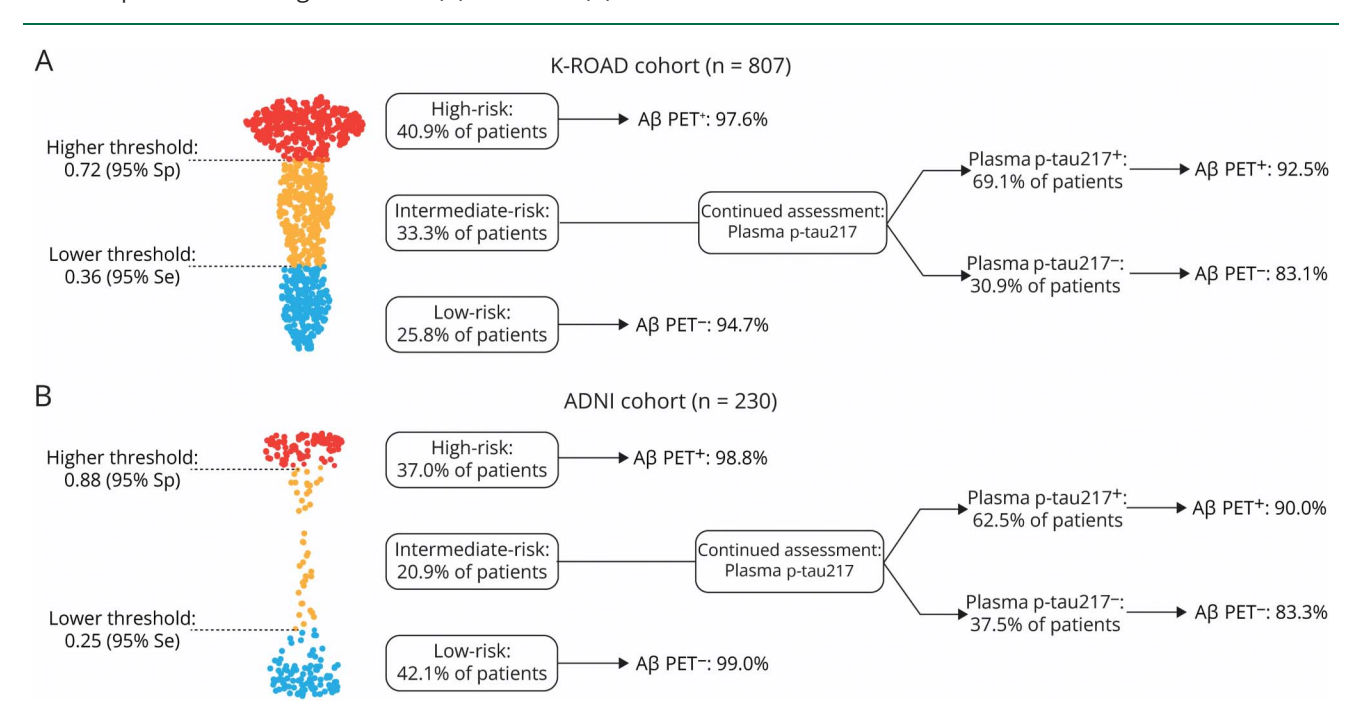
intermediate-risk subgroup, the 2-step approach also significantly improved PPV and NPV (McNemar test, p < 0.01; Figure 5C).

Figure 3 Overall Workflow Accuracy and Cost-Based Approach



(A) The overall accuracy of the 2-step workflow, reflecting the proportion of correct classifications in both low-risk and high-risk groups, along with the accuracy of plasma p-tau217 classifications for the intermediate-risk group, was calculated for the K-ROAD cohort. The error bars correspond to 95% Cls. (B) Bar plots indicating the percentage of the intermediate-risk group by applying the risk stratification strategy, based on each of the risk threshold strategies. (C) The cost estimation for each risk threshold strategy was determined by incorporating additional expenses associated with the plasma p-tau217 test, which was used to assess A $\beta$  PET positivity within the intermediate group. A $\beta$  =  $\beta$ -amyloid; K-ROAD = Korea-Registries to Overcome Dementia and Accelerate Dementia Research.

**Figure 4** Two-Stage Diagnostic Workflow for A $\beta$  (+) on PET Prediction Integrating MRI-Based Risk Stratification and Plasma p-Tau217 Testing in K-ROAD (A) and ADNI (B) Cohorts



The 2-stage diagnostic workflow, based on the 95% Se and 95% Sp threshold strategies, is summarized for the K-ROAD (A) and ANDI (B) cohorts. On the right, the results of the first step, MRI-based risk stratification, are displayed, with red, yellow, and blue dots representing individuals in the high-risk, intermediaterisk, and low-risk groups, respectively. The percentage of A $\beta$  PET positivity in the high-risk group and the percentage of A $\beta$  PET negativity in the low-risk group and the percentage of A $\beta$  PET negativity in the left, the results of the second step, plasma p-tau217 testing conducted exclusively for the intermediate-risk group, are presented. The predictive accuracy for A $\beta$  PET status is represented using the NPV and PPV. A $\beta$  = amyloid- $\beta$ ; ADNI = Alzheimer's Disease Neuroimaging Initiative; K-ROAD = Korea-Registries to Overcome Dementia and Accelerate Dementia Research; NPV = negative predictive value; PPV = positive predictive value; Sp = specificity.

### Discussion

This study used a 2-stage diagnostic workflow combining MRI-based brain atrophy assessments and plasma p-tau217 measurements to stratify individuals with early-stage AD into low-risk, intermediate-risk, and high-risk groups for A $\beta$  PET positivity. Our major findings were as follows. First, MRI-based risk stratification effectively identified individuals at low and high risk of A $\beta$  PET positivity, demonstrating its reliability. Second, plasma p-tau217 testing further refined predictions within the intermediate-risk group, addressing diagnostic uncertainty and enhancing workflow accuracy. Finally, the 2-stage diagnostic workflow, validated using both K-ROAD and ADNI cohorts, highlighted the potential of leveraging routinely collected MRI data to reduce the need for additional biomarker testing, optimizing resource allocation in clinical practice.

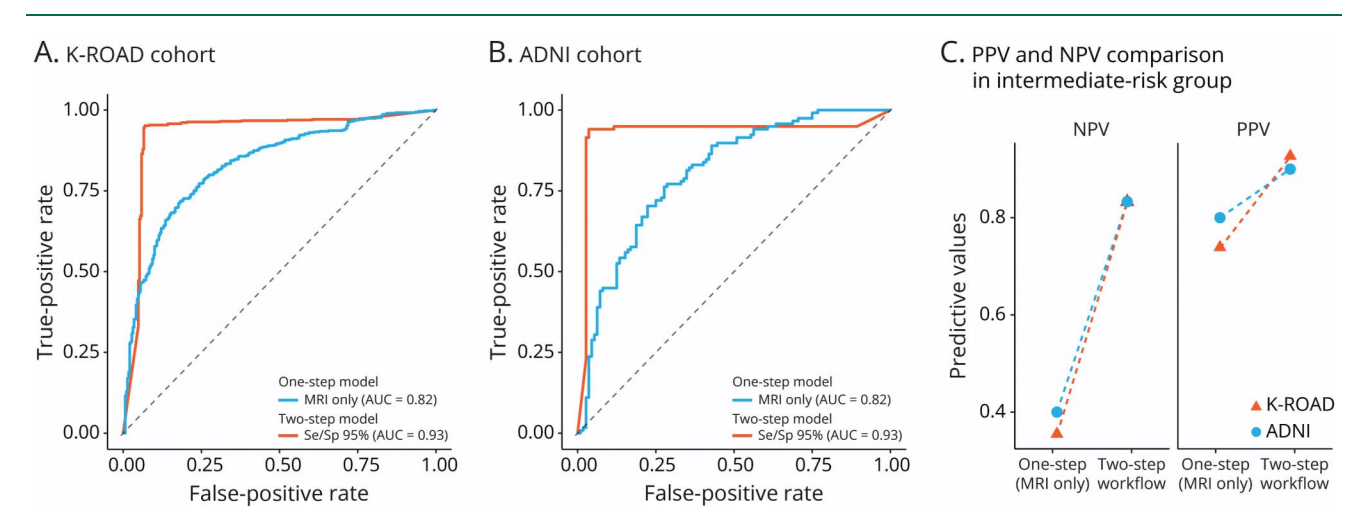
Our first finding showed that MRI-based risk stratification effectively identified A $\beta$  PET-negative individuals in the low-risk group and A $\beta$  PET-positive individuals in the high-risk group, demonstrating its reliability in accurately classifying individuals at both ends of the risk spectrum. This approach was validated in the ADNI cohort, further supporting its generalizability across diverse clinical settings. Regional brain atrophy, particularly in areas such as the medial temporal lobe,

parietal cortex, and precuneus, has been shown to correlate strongly with A $\beta$ -related neurodegeneration. <sup>46</sup> Based on these findings, previous studies have explored MRI-derived structural changes for binary classification of A $\beta$  PET status. <sup>24,47</sup> However, these approaches often fail to address diagnostic uncertainty in intermediate cases, where structural changes may be less distinct. <sup>48,49</sup> Our study's unique contribution lies in its probabilistic framework, which categorizes individuals into distinct risk groups, providing a more nuanced and targeted strategy for resolving diagnostic ambiguity and guiding confirmatory testing or clinical monitoring.

While APOE  $\epsilon$ 4 status was one of the input variables for risk stratification, the observed differences in APOE distribution across risk groups are not solely an artifact of model design but reflect a meaningful biological association. APOE  $\epsilon$  is a well-established genetic risk factor of amyloid accumulation, and its alignment with risk group classification supports the validity of our approach. Additional analyses confirmed that APOE status independently contributes to risk stratification beyond its role as a predictor, reinforcing the robustness of our model (eTable 3).

Our second major finding demonstrated that plasma p-tau217 testing improved predictions within the intermediate-risk group, effectively resolving diagnostic uncertainty and

Figure 5 Model Performance and Predictive Value Across Classification Strategies



ROC curves in the K-ROAD cohort (A) and in the ADNI cohort (B) comparing the 1-step (MRI-only) model and the proposed 2-step model. (C) Comparison of PPV and NPV between the 1-step (MRI-only) and 2-step models in the intermediate-risk group across cohorts. ADNI = Alzheimer's Disease Neuroimaging Initiative; K-ROAD = Korea-Registries to Overcome Dementia and Accelerate Dementia Research; NPV = negative predictive value; PPV = positive predictive value; ROC = receiver operating characteristic.

enhancing overall workflow accuracy. This finding was replicated in the ADNI cohort, confirming the utility of plasma p-tau217 as a complementary biomarker for refining risk stratification across diverse clinical setting. Previous studies have demonstrated that plasma p-tau217 is highly accurate for predicting Aß PET status across entire cohorts, with consistently high concordance rates observed in diverse populations. 30,50,51 However, our findings highlight its robust predictive performance specifically in cases with the greatest diagnostic uncertainty, such as those in the intermediate-risk group. This result emphasizes the biomarker's value in a risk stratification framework, where resolving ambiguity in intermediate-risk groups is critical. By capturing biochemical changes associated with Aß pathology, plasma p-tau217 complements MRI-derived structural data, enhancing the workflow's overall precision. This integration provides a scalable and efficient approach to optimizing diagnostic accuracy and resource allocation in clinical practice. Although sex differences have been reported in AD pathology, our sexstratified analysis demonstrated that the diagnostic accuracy and intermediate-risk proportions were comparable between male and female participants. This finding supports the applicability of our workflow across sexes.

Our final major finding was that leveraging MRI data already collected as part of routine diagnostic evaluations for cognitive impairment significantly reduced the need for additional biomarker testing. To illustrate potential cost savings, we compared our 2-stage workflow with universal PET screening. With amyloid PET positivity rates of 64.3% (K-ROAD) and 52.6% (ADNI), recruiting 1,000 amyloid-positive participants using universal PET would cost approximately USD 6.22 million and USD 7.61 million, respectively (at USD 4,000 per PET scan). By contrast, our workflow reserved PET testing

only for the intermediate-risk group identified by MRI-based stratification (33.3% in K-ROAD; 20.9% in ADNI), who underwent plasma p-tau217 testing at an estimated global market price of USD 300 per test. This significantly reduced additional biomarker testing costs (USD 156,300 in K-ROAD; USD 125,100 in ADNI) while achieving overall accuracies of 94.2% (K-ROAD) and 96.5% (ADNI)—comparable to the performance standards ( $\sim$ 90%) recommended by the CEO Initiative. These results highlight the clinical value of optimizing resource allocation by using MRI, a routine diagnostic tool, to efficiently stratify risk and prioritize biomarker testing for diagnostically uncertain cases. With the increasing availability of amyloid-targeted therapies, identifying amyloid-positive individuals has become essential in early-stage AD management. Our MRI-driven workflow reduces reliance on costly and invasive PET imaging, ensuring that resources are focused effectively on patients most likely to benefit.

A major methodological strength of our study lies in its 2-stage diagnostic workflow, which combines MRI-based risk stratification with plasma biomarker testing to improve diagnostic precision and reduce unnecessary testing in a scalable and clinically practical manner. The two-step approach has traditionally been applied in very low-prevalence conditions, such as HIV screening. More recently, this design has been recognized as an effective strategy to optimize diagnostic precision and resource allocation by reducing unnecessary testing. S2 However, several limitations should be noted. First, although our 2-stage approach significantly improved diagnostic accuracy, the incremental improvement compared with the baseline model was modest, somewhat limiting the clinical impact of our findings. Nevertheless, even modest improvements can be valuable in clinical practice, particularly

given the importance of accurate amyloid detection for patient management and therapeutic decision making. Second, while plasma p-tau217 biomarkers have shown high diagnostic accuracy, the lack of a clear bimodal distribution can lead to overlap between Alzheimer and non-Alzheimer conditions. 53,54 However, our study demonstrated high accuracy of plasma p-tau217 within the intermediate-risk group, mitigating concerns about its diagnostic overlap. Third, the brain atrophy patterns observed in our participants are not entirely specific to AD and can also be seen in other neurodegenerative conditions such as limbic-predominant age-related TDP-43 encephalopathy or hippocampal sclerosis. 26,27,55 Finally, the generalizability of our findings may be limited by the lack of racial and ethnic diversity, as the K-ROAD participants consisted entirely of Korean individuals, and the ADNI participants were predominantly non-Hispanic White. Moreover, the unexpectedly low APOE E4 carrier rate observed in the ADNI cohort may reflect sampling bias or specific inclusion criteria, further limiting generalizability. Future studies incorporating more ethnically diverse populations are needed to validate the applicability of our 2-stage diagnostic workflow across different racial and ethnic groups. Despite these limitations, our study provides valuable insights into the integration of neuroimaging and plasma biomarkers for AD risk stratification. By addressing diagnostic uncertainty in intermediate-risk cases and optimizing resource allocation, the proposed workflow offers a robust framework for improving early diagnosis and advancing clinical care in AD.

In conclusion, this study demonstrates the effectiveness of combining MRI-based risk stratification with plasma biomarker testing to address diagnostic uncertainty and enhance early detection of AD. By leveraging routinely collected imaging data and targeted biomarker testing, this workflow has the potential to improving diagnostic pathways and guiding clinical decision making for patients with early-stage AD.

#### **Author Contributions**

S. Yim: drafting/revision of the manuscript for content, including medical writing for content; analysis or interpretation of data. S. Park: analysis or interpretation of data. K. Lim: major role in the acquisition of data. H. Kang: major role in the acquisition of data. D. Shin: major role in the acquisition of data. Hyunjin Jo: major role in the acquisition of data. H. Jang: major role in the acquisition of data. M.W. Weiner: analysis or interpretation of data. H. Zetterberg: analysis or interpretation of data. K. Blennow: analysis or interpretation of data. F. Gonzalez-Ortiz: analysis or interpretation of data. N.J. Ashton: analysis or interpretation of data. S.H. Kang: major role in the acquisition of data. J. Yun: major role in the acquisition of data. M.Y. Chun: major role in the acquisition of data. E-J Kim: major role in the acquisition of data. H.-J. Kim: major role in the acquisition of data. D.L. Na: major role in the acquisition of data. J.P. Kim: major role in the acquisition of data. S.W. Seo: drafting/revision of the manuscript for content, including medical writing for content; major role in the acquisition of data; study concept or design; analysis or interpretation of data. K. Kwak: drafting/revision of the manuscript for content, including medical writing for content; study concept or design; analysis or interpretation of data.

### **Study Funding**

This research was supported by a grant of the Korea Dementia Research Project through the Korea Dementia Research Center (KDRC), funded by the Ministry of Health & Welfare and the Ministry of Science and ICT, Republic of Korea (RS-2020-KH106434); by the Korea Health Technology R&D Project through the Korea Health Industry Development Institute (KHIDI), funded by the Ministry of Health & Welfare, Republic of Korea (RS-2025-02223212); by the National Research Foundation of Korea (NRF) grant funded by the Korea government (MSIT) (RS-2019-NR040057); by the Institute of Information & Communications Technology Planning & Evaluation (IITP) grant funded by the Korea government (MSIT) (RS-2021-II212068, Artificial Intelligence Innovation Hub); by the Future Medicine 20\*30 Project of Samsung Medical Center (SMX1250081); and by the Korea National Institute of Health research project (2024-ER1003-01). HZ is a Wallenberg Scholar and a Distinguished Professor at the Swedish Research Council supported by grants from the Swedish Research Council (2023-00356, 2022-01018, and 2019-02397); the European Union's Horizon Europe research and innovation programme under grant agreement No. 101053962; Swedish State Support for Clinical Research (ALFGBG-71320); the Alzheimer Drug Discovery Foundation (ADDF), USA (201809-2016862); the AD Strategic Fund and the Alzheimer's Association (ADSF-21-831376-C, ADSF-21-831381-C, 831377-C, and ADSF-24-1284328-C); and the European Partnership on Metrology, co-financed from the European Union's Horizon Europe Research and Innovation Programme, and by the Participating States (NEuroBioStand, 22HLT07); the Bluefield Project; Cure Alzheimer's Fund; the Olav Thon Foundation; the Erling-Persson Family Foundation; Familjen Rönströms Stiftelse, Stiftelsen för Gamla Tjänarinnor, Hjärnfonden, Sweden (FO2022-0270); the European Union's Horizon 2020 research and innovation programme under the Marie Skłodowska-Curie grant agreement No. 860197 (MIRIADE); the European Union Joint - Neurodegenerative Disease Research Programme (JPND2021-00694); the National Institute for Health and Care Research University College London Hospitals Biomedical Research Centre; the UK Dementia Research Institute at UCL (UKDRI-1003); and an anonymous donor.

#### **Disclosure**

S.W. Seo is a co-founder of BeauBrain Healthcare Inc. S. Park, K. Lim, and K. Kwak were employed by BeauBrain Healthcare Inc. H. Zetterberg has served at scientific advisory boards and/or as a consultant for Abbvie, Acumen, Alector, Alzinova, ALZpath, Amylyx, Annexon, Apellis, Artery Therapeutics, AZTherapies, Cognito Therapeutics, CogRx, Denali, Eisai, Enigma, LabCorp, Merry Life, Nervgen, Novo Nordisk,

Optoceutics, Passage Bio, Pinteon Therapeutics, Prothena, Quanterix, Red Abbey Labs, reMYND, Roche, Samumed, Siemens Healthineers, Triplet Therapeutics, and Wave; has given lectures sponsored by Alzecure, BioArctic, Biogen, Cellectricon, Fujirebio, Lilly, Novo Nordisk, Roche, and WebMD; and is a co-founder of Brain Biomarker Solutions in Gothenburg AB (BBS), which is a part of the GU Ventures Incubator Program (outside submitted work). All other authors report no disclosures relevant to the manuscript. Go to Neurology.org/N for full disclosures.

## **Publication History**

Received by *Neurology*® January 22, 2025. Accepted in final form June 18, 2025. Submitted and externally peer reviewed. The handling editor was Assistant Editor Marcello Moccia, MD, PhD and Associate Editor for Editorial Education Bradford Worrall, MD, MSc, FAAN.

### Appendix 1 K-ROAD Coinvestigators

Coinvestigators are listed at Neurology.org.

#### **Appendix 2** ADNI Coinvestigators

Coinvestigators are listed at Neurology.org.

#### References

- Scheltens P, Blennow K, Breteler MM, et al. Alzheimer's disease. Lancet. 2016; 388(10043):505-517. doi:10.1016/S0140-6736(15)01124-1
- Bloom GS. Amyloid-beta and tau: the trigger and bullet in Alzheimer disease pathogenesis. JAMA Neurol. 2014;71(4):505-508. doi:10.1001/jamaneurol.2013.5847
- Wang L, Benzinger TL, Su Y, et al. Evaluation of tau imaging in staging alzheimer disease and revealing interactions between beta-amyloid and tauopathy. JAMA Neurol. 2016;73(9):1070-1077. doi:10.1001/jamaneurol.2016.2078
- Zhang H, Wei W, Zhao M, et al. Interaction between Aβ and tau in the pathogenesis of Alzheimer's disease. Int J Biol Sci. 2021;17(9):2181-2192. doi:10.7150/ijbs.57078
- Jarholm JA, Bjørnerud A, Dalaker TO, et al. Medial temporal lobe atrophy in predementia Alzheimer's disease: a longitudinal multi-site study comparing staging and A/T/N in a clinical research cohort. J Alzheimers Dis. 2023;94(1):259-279. doi: 10.3233/JAD-221274
- Chauveau L, Kuhn E, Palix C, et al. Medial temporal lobe subregional atrophy in aging and Alzheimer's disease: a longitudinal study. Front Aging Neurosci. 2021;13:750154. doi:10.3389/fnagi.2021.750154
- Jobst KA, Smith AD, Barker CS, et al. Association of atrophy of the medial temporal lobe with reduced blood flow in the posterior parietotemporal cortex in patients with a clinical and pathological diagnosis of Alzheimer's disease. J Neurol Neurosurg Psychiatry. 1992;55(3):190-194. doi:10.1136/jnnp.55.3.190
- Buckner RL, Snyder AZ, Shannon BJ, et al. Molecular, structural, and functional characterization of Alzheimer's disease: evidence for a relationship between default activity, amyloid, and memory. J Neurosci. 2005;25(34):7709-7717. doi:10.1523/ INEUROSCI.2177-05.2005
- Nestor SM, Rupsingh R, Borrie M, et al. Ventricular enlargement as a possible measure of Alzheimer's disease progression validated using the Alzheimer's disease neuroimaging initiative database. *Brain*. 2008;131(pt 9):2443-2454. doi:10.1093/ brain/awn146
- Mintun MA, Lo AC, Duggan Evans C, et al. Donanemab in early Alzheimer's disease. N Engl J Med. 2021;384(18):1691-1704. doi:10.1056/NEJMoa2100708
- van Dyck CH, Swanson CJ, Aisen P, et al. Lecanemab in early Alzheimer's disease. N Engl J Med. 2023;388(1):9-21. doi:10.1056/NEJMoa2212948
- Lowe VJ, Mester CT, Lundt ES, et al. Amyloid PET detects the deposition of brain Aβ earlier than CSF fluid biomarkers. Alzheimers Dement. 2024;20(11):8097-8112. doi: 10.1002/alz.14317
- Zammit MD, Tudorascu DL, Laymon CM, et al. PET measurement of longitudinal amyloid load identifies the earliest stages of amyloid-beta accumulation during Alzheimer's disease progression in Down syndrome. Neuroimage. 2021;228:117728. doi: 10.1016/j.neuroimage.2021.117728
- Mattsson N, Palmqvist S, Stomrud E, Vogel J, Hansson O. Staging beta-amyloid pathology with amyloid positron emission tomography. *JAMA Neurol.* 2019;76(11): 1319-1329. doi:10.1001/jamaneurol.2019.2214

- Mattsson-Carlgren N, Andersson E, Janelidze S, et al. Aβ deposition is associated with increases in soluble and phosphorylated tau that precede a positive tau PET in Alzheimer's disease. Sci Adv. 2020;6(16):eaaz2387. doi:10.1126/sciadv.aaz2387
- Palmqvist S, Zetterberg H, Blennow K, et al. Accuracy of brain amyloid detection in clinical practice using cerebrospinal fluid beta-amyloid 42: a cross-validation study against amyloid positron emission tomography. JAMA Neurol. 2014;71(10): 1282-1289. doi:10.1001/jamaneurol.2014.1358
- Cicognola C, Brinkmalm G, Wahlgren J, et al. Novel tau fragments in cerebrospinal fluid: relation to tangle pathology and cognitive decline in Alzheimer's disease. Acta Neuropathol. 2019;137(2):279-296. doi:10.1007/s00401-018-1948-2
- Johnson KA, Fox NC, Sperling RA, Klunk WE. Brain imaging in Alzheimer disease.
  Cold Spring Harb Perspect Med. 2012;2(4):a006213. doi:10.1101/cshperspect.a006213
- Duits FH, Martinez-Lage P, Paquet C, et al. Performance and complications of lumbar puncture in memory clinics: results of the multicenter lumbar puncture feasibility study. Alzheimers Dement. 2016;12(2):154-163. doi:10.1016/j.jalz.2015.08.003
- Tartaglia MC, Rosen HJ, Miller BL. Neuroimaging in dementia. Neurotherapeutics. 2011;8(1):82-92. doi:10.1007/s13311-010-0012-2
- Masdeu JC, Pascual B. Neuroimaging of disorders leading to dementia. Curr Neurol Neurosci Rep. 2008;8(6):443-444. doi:10.1007/s11910-008-0069-z
- Chételat G, Villemagne VL, Villain N, et al. Accelerated cortical atrophy in cognitively normal elderly with high beta-amyloid deposition. *Neurology*. 2012;78(7):477-484. doi:10.1212/WNL.0b013e318246d67a
- Nosheny RL, Insel PS, Mattsson N, et al. Associations among amyloid status, age, and longitudinal regional brain atrophy in cognitively unimpaired older adults. Neurobiol Aging. 2019;82:110-119. doi:10.1016/j.neurobiolaging.2019.07.005
- Chun MY, Kim GH, Park HK, et al. Predictive scale for amyloid PET positivity based on clinical and MRI variables in patients with amnestic mild cognitive impairment. J Clin Med. 2022;11(12):3433. doi:10.3390/jcm11123433
- Kang SH, Cheon BK, Kim JS, et al. Machine learning for the prediction of amyloid positivity in amnestic mild cognitive impairment. J Alzheimers Dis. 2021;80(1): 143-157. doi:10.3233/JAD-201092
- van de Pol LA, Hensel A, Barkhof F, Gertz HJ, Scheltens P, van der Flier WM. Hippocampal atrophy in Alzheimer disease: age matters. Neurology. 2006;66(2): 236-238. doi:10.1212/01.wnl.0000194240.47892.4d
- Barkhof F, Polvikoski TM, van Straaten EC, et al. The significance of medial temporal lobe atrophy: a postmortem MRI study in the very old. Neurology. 2007;69(15): 1521-1527. doi:10.1212/01.wnl.0000277459.83543.99
- Wolz R, Julkunen V, Koikkalainen J, et al. Multi-method analysis of MRI images in early diagnostics of Alzheimer's disease. PLoS One. 2011;6(10):e25446. doi:10.1371/ journal.pone.0025446
- Van Poppel H, Hogenhout R, Albers P, van den Bergh RCN, Barentsz JO, Roobol MJ.
  A European model for an organised risk-stratified early detection programme for prostate cancer. Eur Urol Oncol. 2021;4(5):731-739. doi:10.1016/j.euo.2021.06.006
- Palmqvist S, Janelidze S, Quiroz YT, et al. Discriminative accuracy of plasma phosphotau217 for alzheimer disease vs other neurodegenerative disorders. *JAMA*. 2020; 324(8):772-781. doi:10.1001/jama.2020.12134
- Milà-Alomà M, Ashton NJ, Shekari M, et al. Plasma p-tau231 and p-tau217 as state markers of amyloid-beta pathology in preclinical Alzheimer's disease. Nat Med. 2022; 28(9):1797-1801. doi:10.1038/s41591-022-01925-w
- De Meyer S, Schaeverbeke JM, Luckett ES, et al. Plasma pTau181 and pTau217 predict asymptomatic amyloid accumulation equally well as amyloid PET. Brain Commun. 2024;6(4):fcae162. doi:10.1093/braincomms/fcae162
- Jack CR, Wiste HJ, Algeciras-Schimnich A, et al. Predicting amyloid PET and tau PET stages with plasma biomarkers. *Brain*. 2023;146(5):2029-2044. doi:10.1093/brain/ awad042
- Jang H, Shin D, Kim Y, et al. Korea-Registries to Overcome Dementia and Accelerate Dementia Research (K-ROAD): a cohort for dementia research and ethnic-specific insights. Dement Neurocogn Disord. 2024;23(4):212-223. doi:10.12779/ dnd.2024.23.4.212
- Ryu HJ, Yang DW. The Seoul Neuropsychological Screening Battery (SNSB) for comprehensive neuropsychological assessment. *Dement Neurocogn Disord*. 2023;22: 1-15. doi:10.12779/dnd.2023.22.1.1
- Petersen RC, Smith GE, Waring SC, Ivnik RJ, Tangalos EG, Kokmen E. Mild cognitive impairment: clinical characterization and outcome. Arch Neurol. 1999;56(3): 303-308. doi:10.1001/archneur.56.3.303
- Albert MS, DeKosky ST, Dickson D, et al. The diagnosis of mild cognitive impairment due to Alzheimer's disease: recommendations from the National Institute on Aging-Alzheimer's Association workgroups on diagnostic guidelines for Alzheimer's disease. Alzheimers Dement. 2011;7(3):270-279. doi:10.1016/j.jalz.2011.03.008
- McKhann GM, Knopman DS, Chertkow H, et al. The diagnosis of dementia due to Alzheimer's disease: recommendations from the National Institute on Aging-Alzheimer's Association workgroups on diagnostic guidelines for Alzheimer's disease. Alzheimers Dement. 2011;7(3):263-269. doi:10.1016/j.jalz.2011.03.005
- Fazekas F, Chawluk JB, Alavi A, Hurtig HI, Zimmerman RA. MR signal abnormalities at 1.5 T in Alzheimer's dementia and normal aging. AJR Am J Roentgenol. 1987; 149(2):351-356. doi:10.2214/ajr.149.2.351
- Alzheimer's Disease Neuroimaging Initiative (ADNI). Accessed July 26, 2025. https://adni-info.org.
- Global Alzheimer's Association Interactive Network (GAAIN). Accessed July 26, 2025. https://www.gaain.org/.
- ADNI. Image data and methods. Accessed July 26, 2025. https://adni.loni.usc.edu/ methods/.

- Isensee F, Jaeger PF, Kohl SAA, Petersen J, Maier-Hein KH. nnU-Net: a selfconfiguring method for deep learning-based biomedical image segmentation. Nat Methods. 2021;18(2):203-211. doi:10.1038/s41592-020-01008-z
- R Core Team. R: A language and environment for statistical computing. Accessed July 26, 2025. https://www.r-project.org.
- Scikit-learn: Machine learning in Python. Accessed July 26, 2025. https://scikit-learn. org/stable/index.html.
- Tosun D, Schuff N, Mathis CA, Jagust W, Weiner MW; Alzheimer's Disease NeuroImaging Initiative. Spatial patterns of brain amyloid-beta burden and atrophy rate associations in mild cognitive impairment. Brain. 2011;134(pt 4):1077-1088. doi:10.1093/brain/awr044
- Pekkala T, Hall A, Ngandu T, et al. Detecting amyloid positivity in elderly with increased risk of cognitive decline. Front Aging Neurosci. 2020;12:228. doi:10.3389/ fnagi.2020.00228
- Loreto F, Gontsarova A, Scott G, et al. Visual atrophy rating scales and amyloid PET status in an Alzheimer's disease clinical cohort. Ann Clin Transl Neurol. 2023;10(4): 619-631. doi:10.1002/acn3.51749
- Imabayashi E, Ishii K, Toyohara J, et al. Possibility of enlargement in left medial temporal areas against cerebral amyloid deposition observed during preclinical stage. Front Aging Neurosci. 2022;14:847094. doi:10.3389/fnagi.2022.847094

- Asken BM, DeSimone JC, Wang WE, et al. Plasma p-tau217 concordance with amyloid PET among ethnically diverse older adults. Alzheimers Dement (Amst). 2024; 16(3):e12617. doi:10.1002/dad2.12617
- Molina-Henry D, Langford O, Donohue MC, et al. Relationship between plasma P-Tau217 and amyloid PET in racial and ethnic underrepresented groups (RE-URG) compared with non RE-URG in LEARN and A4. J Prev Alzheimers Dis. 2024;11(4): 831-837. doi:10.14283/jpad.2024.124
- Brum WS, Cullen NC, Janelidze S, et al. A two-step workflow based on plasma p-tau217 to screen for amyloid beta positivity with further confirmatory testing only in uncertain cases. Nat Aging. 2023;3(9):1079-1090. doi:10.1038/s43587-023-00471-5
- Karikari TK, Ashton NJ, Brinkmalm G, et al. Blood phospho-tau in Alzheimer disease: analysis, interpretation, and clinical utility. Nat Rev Neurol. 2022;18(7):400-418. doi: 10.1038/s41582-022-00665-2
- Therriault J, Servaes S, Tissot C, et al. Equivalence of plasma p-tau217 with cerebrospinal fluid in the diagnosis of Alzheimer's disease. Alzheimers Dement. 2023; 19(11):4967-4977. doi:10.1002/alz.13026
- Butler Pagnotti RM, Pudumjee SB, Cross CL, Miller JB. Cognitive and clinical characteristics of patients with limbic-predominant age-related TDP-43 encephalopathy. Neurology. 2023;100(19):e2027-e2035. doi:10.1212/WNL.0000000000207159